

## Orthorhombic anisotropy: A physical model study

Scott P. Cheadle, R. James Brown and Don C. Lawton

### ABSTRACT

An industrial laminate has been shown to possess anisotropy when used as a medium for the propagation of elastic waves. The material, Phenolic CE, is composed of thin layers of canvas fabric with an approximately orthogonal weave of fibers bonded with a phenolic resin. Different compressional-wave velocities and distinct patterns of shear-wave splitting are observed in experiments involving ultrasonic transmission in three mutually orthogonal (principal) directions through a cube of the material, as well as between edges of the cube beveled at  $45^\circ$  to the adjacent principal axes. Analysis of the results demonstrates that the phenolic laminate is suitable for modeling media with anisotropy of orthorhombic symmetry. The  $P$ -wave anisotropy varies from 6.3% to 22.4% and the  $S$ -wave anisotropy from 3.5% to 9.6% between pairs of the three principal axes. Expressions are presented that relate the measured body-wave velocities to nine elastic coefficients that define the stiffness matrix for this case of orthorhombic symmetry.

### INTRODUCTION

Shear-wave splitting and anisotropy are being studied by more and more people worldwide as part of the ongoing effort to enhance seismic data interpretation and reservoir exploitation. Multicomponent surface-seismic, VSP, crosswell and full-waveform sonic data are being used to determine the relationships among anisotropy, shear-wave polarization and fracture patterns (Keith and Crampin, 1977; Crampin, 1981, 1984, 1985; Lewis et al., 1989, Yale and Sprunt, 1989). Banik (1984) reported errors in depth estimates of between 150 and 300 m in areas of the North Sea basin due to anisotropy within some shaly units. Ensley (1989) described anisotropy values of between -40% and +40% for "sand-, shale- and carbonate-prone" units in the Prudhoe Bay area. Both compressional- and shear-wave anisotropy impact on velocity analysis for multicomponent imaging and methods of estimating stress based on the  $V_s/V_p$  ratio (Thomsen, 1986, 1988). Liu et al. (1989) have used numerical modeling results to outline the potential and limitations of shear-wave splitting analysis in the crosswell configuration. Tatham et al. (1987) and Ebrom et al. (1990) described physical modeling experiments simulating fracture-induced azimuthal anisotropy.

Physical modeling studies of anisotropy are being conducted as part of the CREWES Project (Consortium for Research in Elastic Wave Exploration Seismology) at the University of Calgary. Ultrasonic modeling using phenolic laminate is ideally suited to the study of velocity anisotropy because the ambiguities inherent in field data are absent. To proceed, the parameters that characterize the modeling material must first be measured. This paper describes the results of experiments to determine the anisotropic elastic properties of Phenolic CE.

Based on our initial observations of shear-wave splitting and velocity measurements at various directions through a cube of the phenolic, it seems clear to us that this material can be described, to a high degree of accuracy, as possessing three mutually orthogonal axes of twofold symmetry. This is the same symmetry exhibited by the orthorhombic class of crystals. The elastic properties of such anisotropic crystals have been studied extensively (Fedorov, 1968; e.g. Musgrave, 1970; Nye, 1985). The theory of wave propagation in anisotropic media is used to

relate the nine elastic stiffnesses (orthorhombic case) to observed body-wave velocities, permitting one to compute the details of elastic-wave propagation in any direction through the phenolic.

## PHYSICAL MODEL EXPERIMENTS

We are using piezoelectric *P*-wave and *S*-wave transducers as both sources and receivers in our multicomponent physical modeling. Both types are flat-faced cylindrical contact transducers with an active element 12.6 mm in diameter. The compressional or *P*-wave transducer (Panametrics V103) is vertically polarized, with the maximum sensitivity normal to the contact face. The shear-wave transducer (Panametrics V153) is horizontally polarized, with the maximum sensitivity parallel to a line across the contact face. During operation, these contact faces are coupled to a selected flat surface of the phenolic and, for a particular experiment, a profile direction and sagittal plane are established. To record the radial component, the shear receiver transducer is used with the polarization parallel to the direction of the profile (in-line), whereas for the transverse component, the transducers are rotated so that the polarization is perpendicular to the azimuth of the profile and to the sagittal plane (cross-line).

The source transducer is driven with a 28-volt square wave tuned to produce a broadband wavelet with a central frequency of 600 kHz. Amplified data are sampled using a Nicolet digital oscilloscope connected, through an IBM-XT which controls the experiments, to a Perkin-Elmer 3220 seismic processing system for storage. Traces of up to 4096 samples are recorded sequentially and stored on tape or disc in SEG-Y format.

The CE-grade phenolic laminate is composed of layers of a woven canvas fabric saturated and bonded with a phenolic resin, and has a density of 1364 kg/m<sup>3</sup>. Initial tests with the material showed a directional dependence of the velocity for both *P* and *S* waves, suggesting its suitability for physical modeling of an anisotropic medium. Shear-wave splitting was observed during transmission tests when the sample was rotated between two shear-wave transducers. The polarizations of the split shear waves were approximately parallel to the orientations of the orthogonal weave of fibers in the canvas fabric. For this reason, subsequent experiments were conducted on pieces of phenolic that were cut with faces parallel or orthogonal to the observed fiber directions as well as to the plane of the canvas layers.

### Shear-wave splitting

Shear-wave splitting experiments were conducted using cubes of phenolic. A sample of the CE grade phenolic with the faces labeled with the convention used in this study is shown in Figure 1. The factory-machined surface of the laminate sheet, parallel to the fabric layers, was designated Face 3, consistent with the conventional choice of  $x_3$  as the vertical direction and with a horizontal attitude for the layering of the medium. The other two sides of the cube were designated Faces 1 and 2. The 1-direction is therefore the normal with respect to Face 1 and likewise for the 2- and 3-directions. Since the 3-direction turned out to be the slowest for *P*-wave propagation, the other two principal directions were labelled such that the 1-direction is fastest and the 2-direction intermediate for *P*-wave propagation.

The apparatus used for studying split shear waves is shown in Figure 2. The cube of material is placed between two fixed shear-wave transducers which are aligned with parallel polarizations. The cube is rotated between the transducers, and a pointer on the cube is used to determine the azimuth of the sample with respect to a fixed circular protractor. A similar experimental procedure was described by Tatham et al. (1987) for a study of fracture-induced shear-wave splitting.

Figures 3, 4 and 5 show the transmission records through Faces 1, 2 and 3, respectively, of an approximately 9.6 cm cube of phenolic. Each trace records the signal transmitted through the

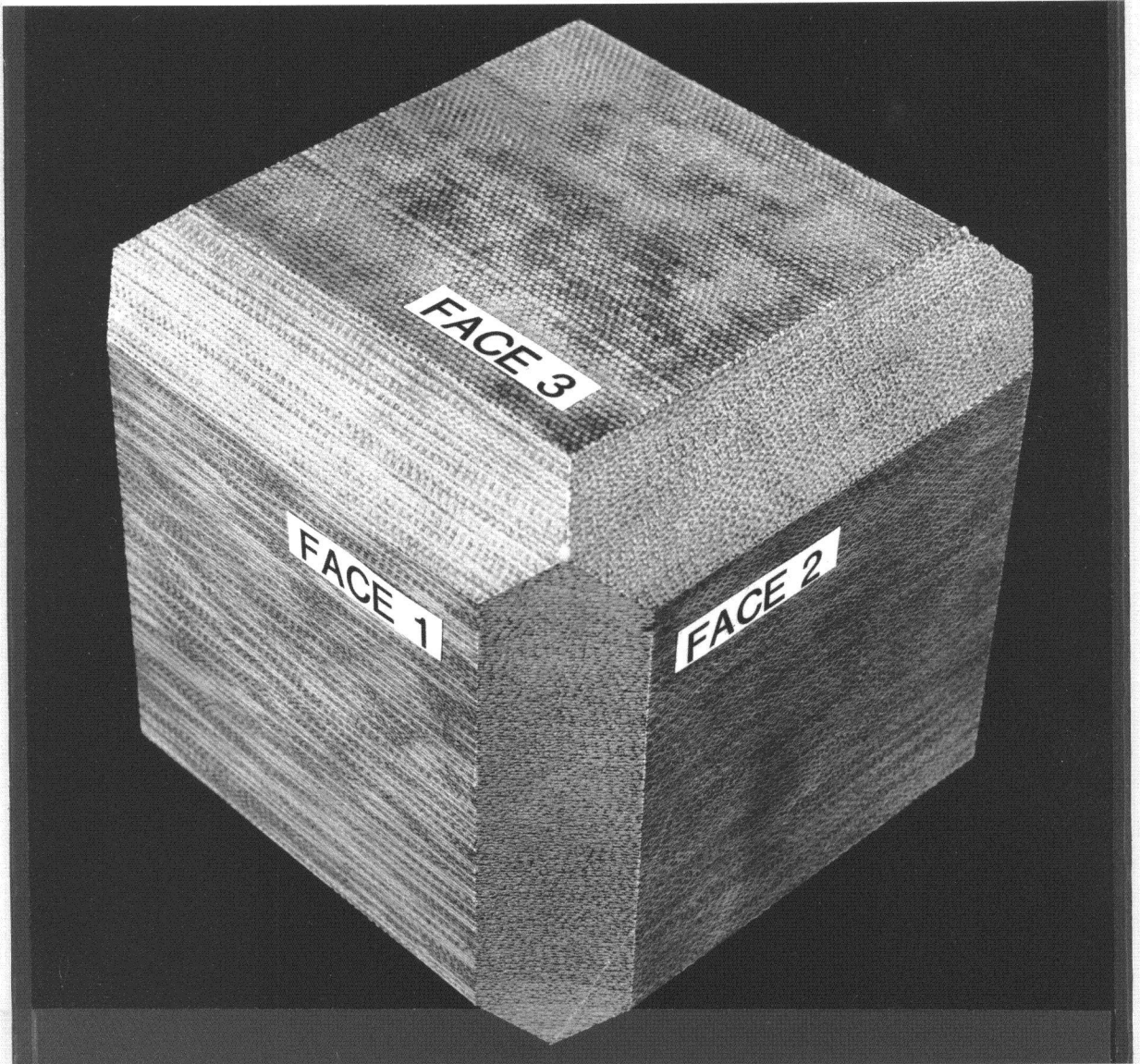


Fig. 1. Phenolic CE laminate is composed of layers of a canvas weave fabric bonded with phenolic resin. The faces are labeled as used in this study.

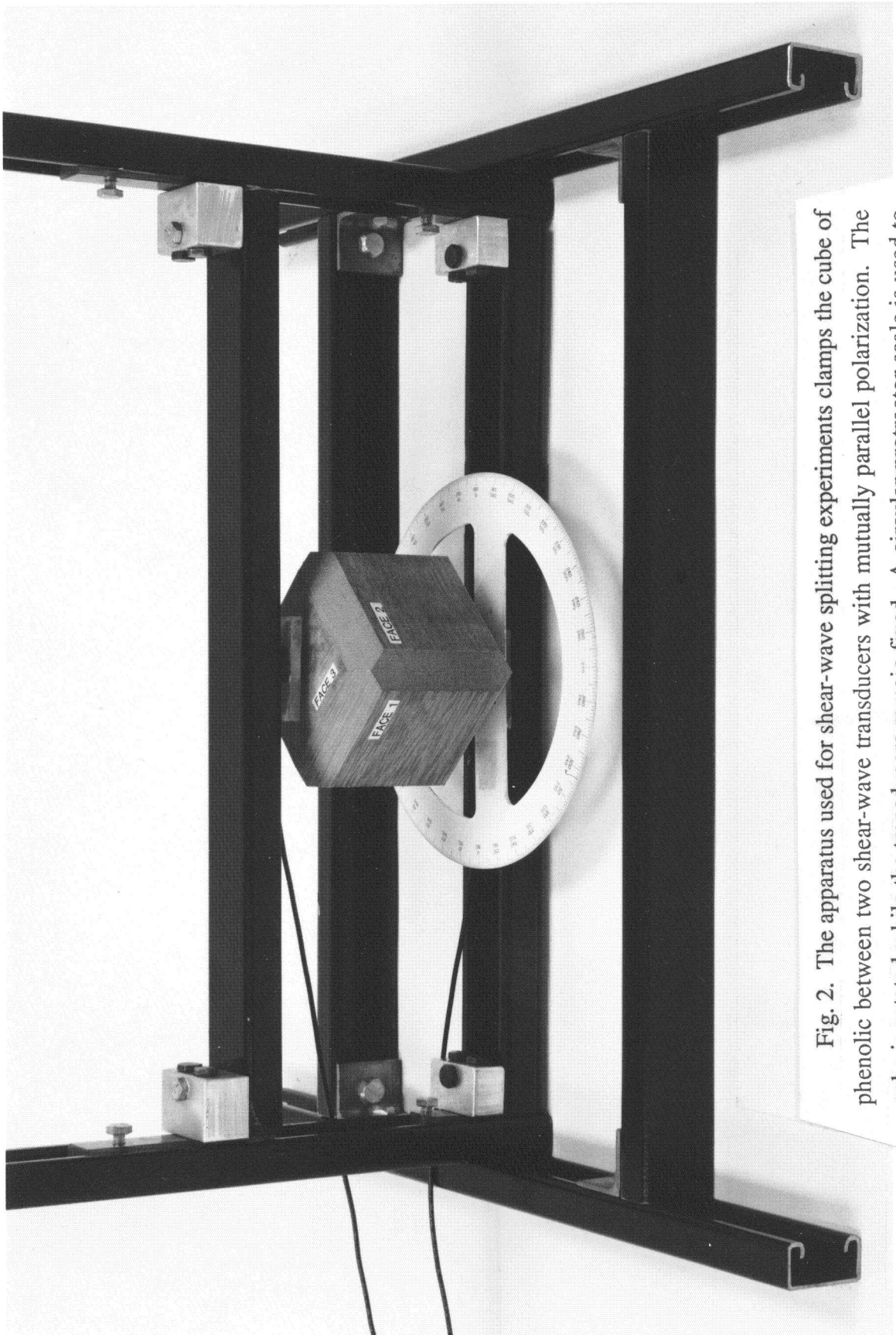


Fig. 2. The apparatus used for shear-wave splitting experiments clamps the cube of phenolic between two shear-wave transducers with mutually parallel polarization. The cube is rotated while the transducers remain fixed. A circular protractor scale is used to determine the azimuth of rotation.

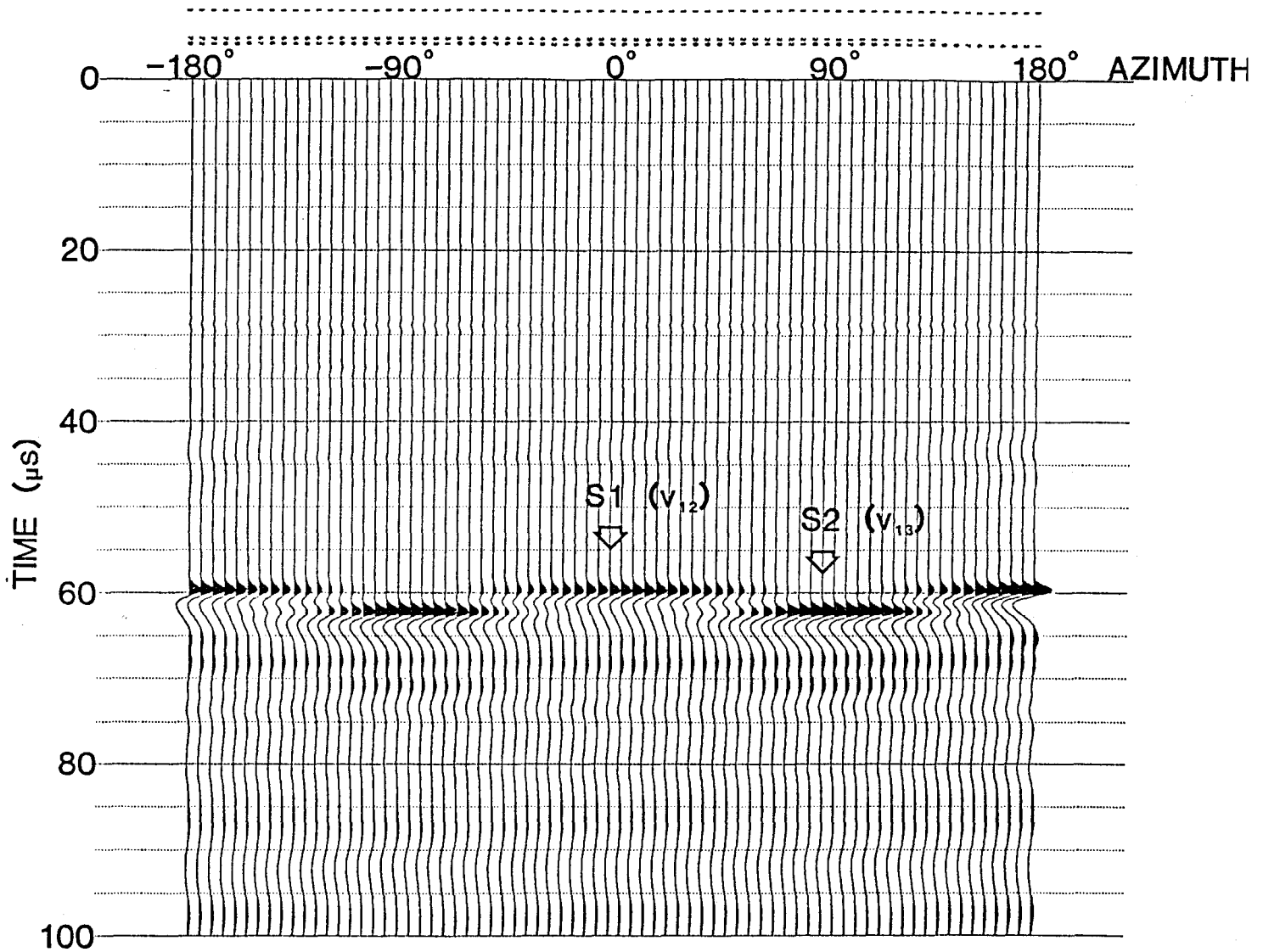


Fig. 3. The record through Face 1 of a 9.6 cm cube of phenolic, showing the faster  $S_1$  arrival at 1665 m/s and the slower  $S_2$  arrival at 1602 m/s. The compressional velocity in the 1-direction is 3576 m/s. The polarization direction of the  $S_1$  amplitude maximum is parallel to the "bedding plane" of the canvas layers, while that of the  $S_2$  amplitude maximum is perpendicular to that plane.

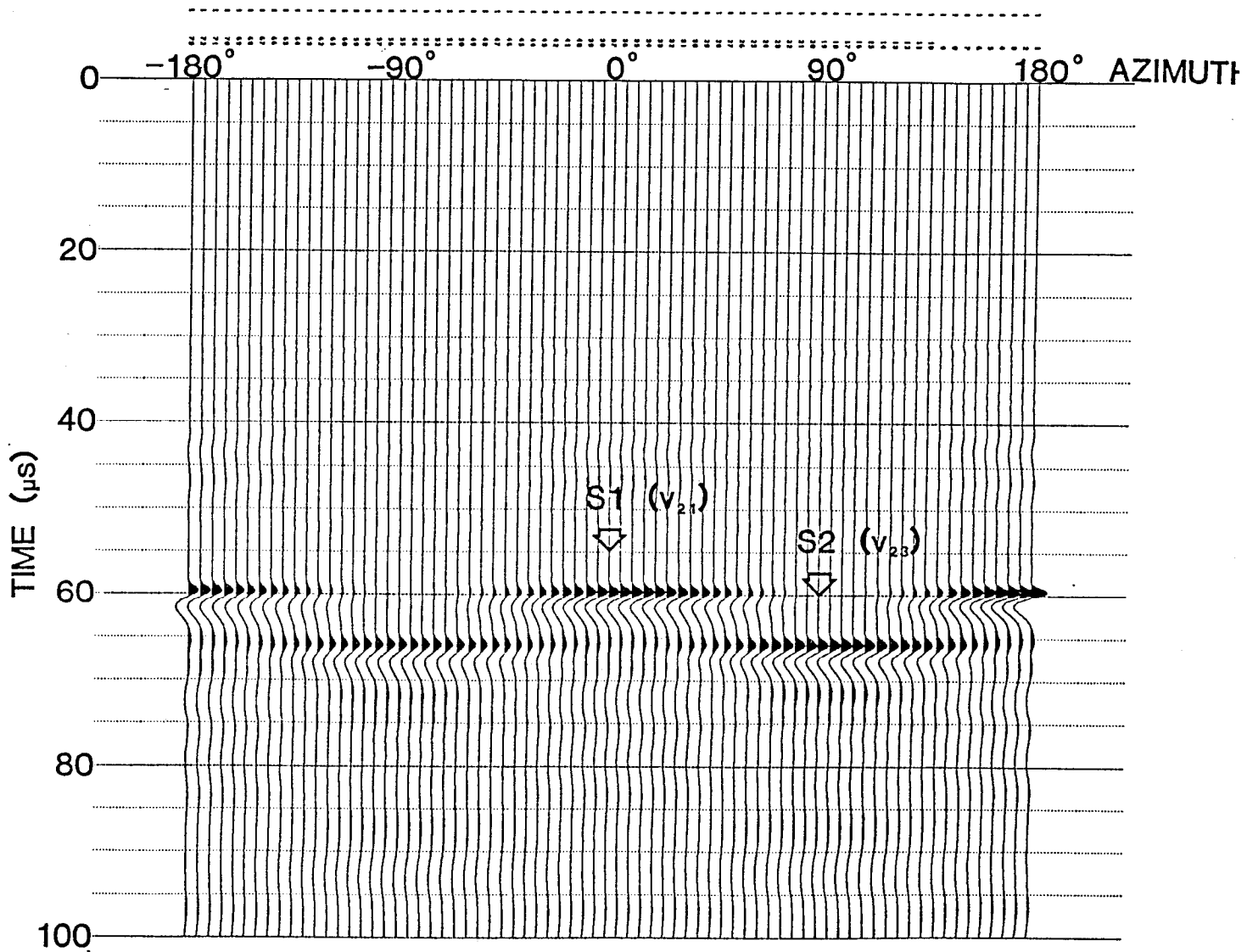


Fig. 4. The record through Face 2, showing the faster  $S_1$  arrival at 1658 m/s and the slower  $S_2$  arrival at 1506 m/s. The compressional velocity in the 2-direction is 3365 m/s. The polarization directions of the  $S_1$  and  $S_2$  amplitude maxima are parallel and perpendicular respectively to the canvas layering, as in Fig. 3.

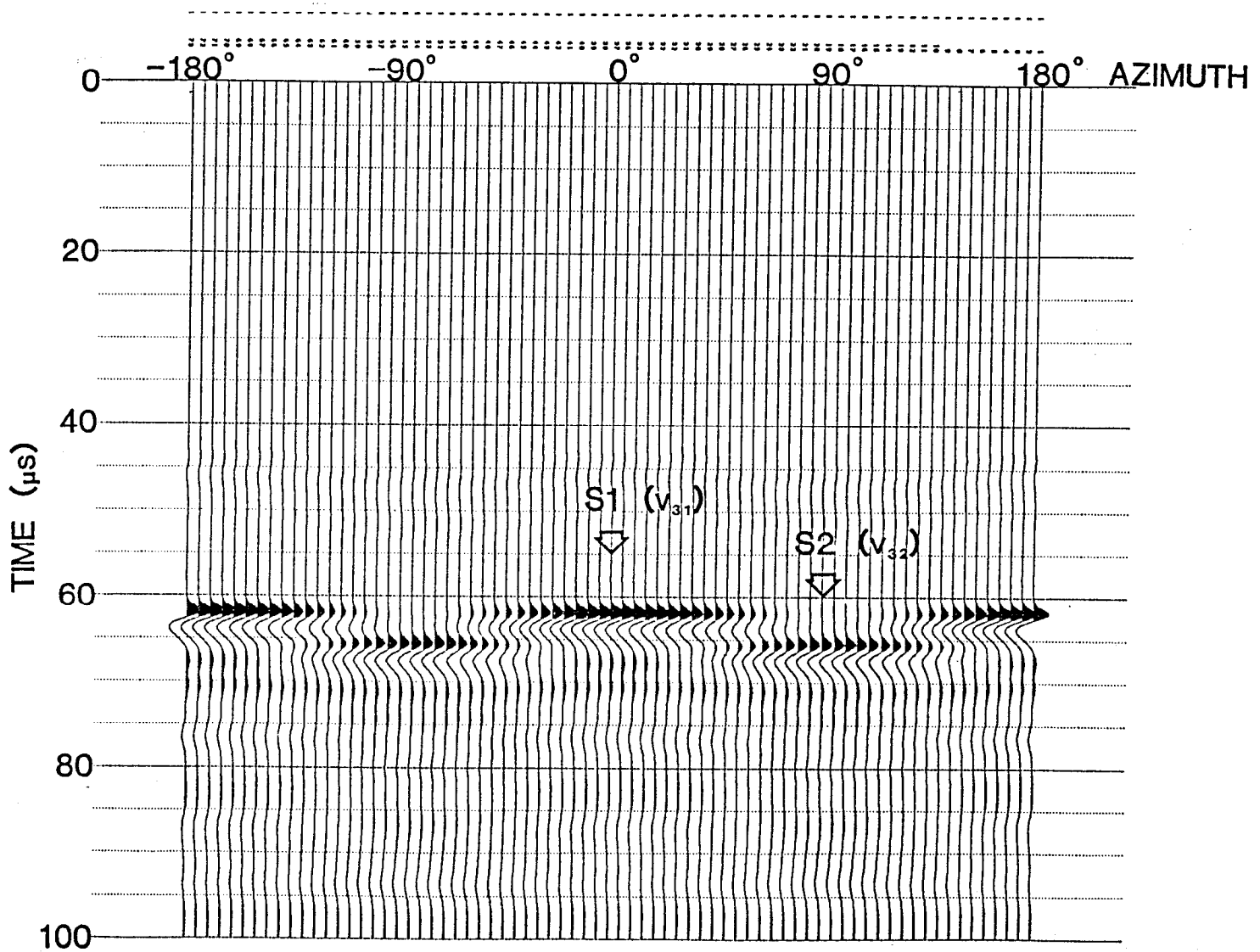


Fig. 5. The record through Face 3, showing the faster  $S_1$  (1610 m/s) and slower  $S_2$  (1525 m/s) shear waves. The compressional velocity in the 3-direction, determined separately with P-wave transducers, is 2925 m/s. The traces for the records of Fig. 3 - 5 were recorded at  $5^\circ$  intervals of rotation.

cube at 5° intervals of rotation with respect to the polarization direction of the shear-wave transducers. The 0° direction was chosen to correspond to the azimuth of the amplitude maximum of the faster of the two shear-wave arrivals. The sample interval used in this study was 50 nanoseconds, and the arrival times are shown in microseconds. The faster shear arrival is designated  $S_1$  and the slower mode  $S_2$ . While it is more correct to refer to the split shear waves and the compressional waves under most conditions as quasishear and quasicompressional modes, except for special cases, such as propagation in one of the principal directions, that prefix will be implied rather than included where appropriate. On Figures 3, 4 and 5, the weakly coupled  $P$ -wave arrival is barely visible. The compressional velocities were determined separately using the  $P$ -wave transducers.

On Figures 3 and 4, in the 1-and 2-directions, respectively, the polarizations at the  $S_1$  amplitude maxima are, in each case, parallel to the "bedding plane" of the canvas layers, whereas for the  $S_2$  amplitude maxima, the polarizations are perpendicular to this plane. In Figure 5, for propagation in the 3-direction, the polarization of the  $S_1$  amplitude maximum is parallel to the 1-direction (one of the fiber directions), while the  $S_2$  amplitude maximum is parallel to the 2-direction (the other fiber direction). A plot of amplitude vs. polarization direction for a record through Face 2 is shown in Figure 6. This and other transmission records through the phenolic show that the  $S_1$  mode generally has a greater maximum amplitude than the  $S_2$  arrival, indicating that the effective attenuation is also dependent on the polarization direction. The ratios of the amplitudes of the  $S_1$  arrivals to those of the  $S_2$  arrivals, measured at their maxima, have ranged from 1.1 to 1.4 for the samples tested.

The  $P$ ,  $S_1$  and  $S_2$  velocities measured along the principal axes are summarized in Figure 7 and those along the diagonals (between opposing edges) in Figure 8. The values quoted are group velocities based on the transit time measured with respect to the onset of the pulse. The velocities are the averages of values measured through 10 cm and 8 cm cubes. The measured velocities for the phenolic cubes were repeatable to within  $\pm 15$  m/s ( $\approx 0.5\%$ ) for  $P$ -waves and  $\pm 4$  m/s ( $\approx 0.25\%$ ) for shear waves. The variations are likely related to small inconsistencies in the thickness of the coupling agent used to bond the transducers to the phenolic. Velocity variations between different samples of phenolic ranged up to 2%. The time picks used to calculate the velocities were made directly on the digital oscilloscope for maximum accuracy.

For the following discussion, the velocities will be labeled with 2 subscripts indicating the directions of propagation and polarization (i.e. particle motion) with respect to the three principal axes. For example,  $V_{11}$  is the group velocity for propagation and particle motion in the 1-direction ( $P$ -wave) while  $V_{12}$  indicates propagation in the 1-direction with polarization in the 2 direction ( $S$ -wave). For the cases of the diagonal raypaths we adopt in this paper a special index convention. For propagation in the 23-plane with the ray direction at 45° to the 2-and 3-directions we use the index 4. The group velocity of the quasi- $P$  wave in this direction is designated by  $V_{44}$ , while the group velocity of the  $S$  wave with particle motion in the 23-plane, i.e. the quasi- $SV$ , is designated  $V_{44}$ . The velocity of the corresponding  $SH$  wave, with particle motion in the 1-direction, is labelled  $V_{41}$ . Similarly, we use the indices 5 and 6 to denote propagation in the 31- and 12-planes, respectively, with the ray direction bisecting the respective axial directions. The  $P$ -,  $SV$ - and  $SH$ -wave group velocities are thus labeled  $V_{55}$ ,  $V_{55}$  and  $V_{52}$ , in the 31-plane, and  $V_{66}$ ,  $V_{66}$  and  $V_{63}$ , in the 12-plane.

Slow, medium and fast directions through the cube (3, 2 and 1, respectively) were defined on the basis of the compressional velocities. Of the six shear-wave velocities measured in the principal directions there are, according to orthorhombic theory (Appendix), three independent values, which depend on the direction of propagation and particle motion. To a high degree of

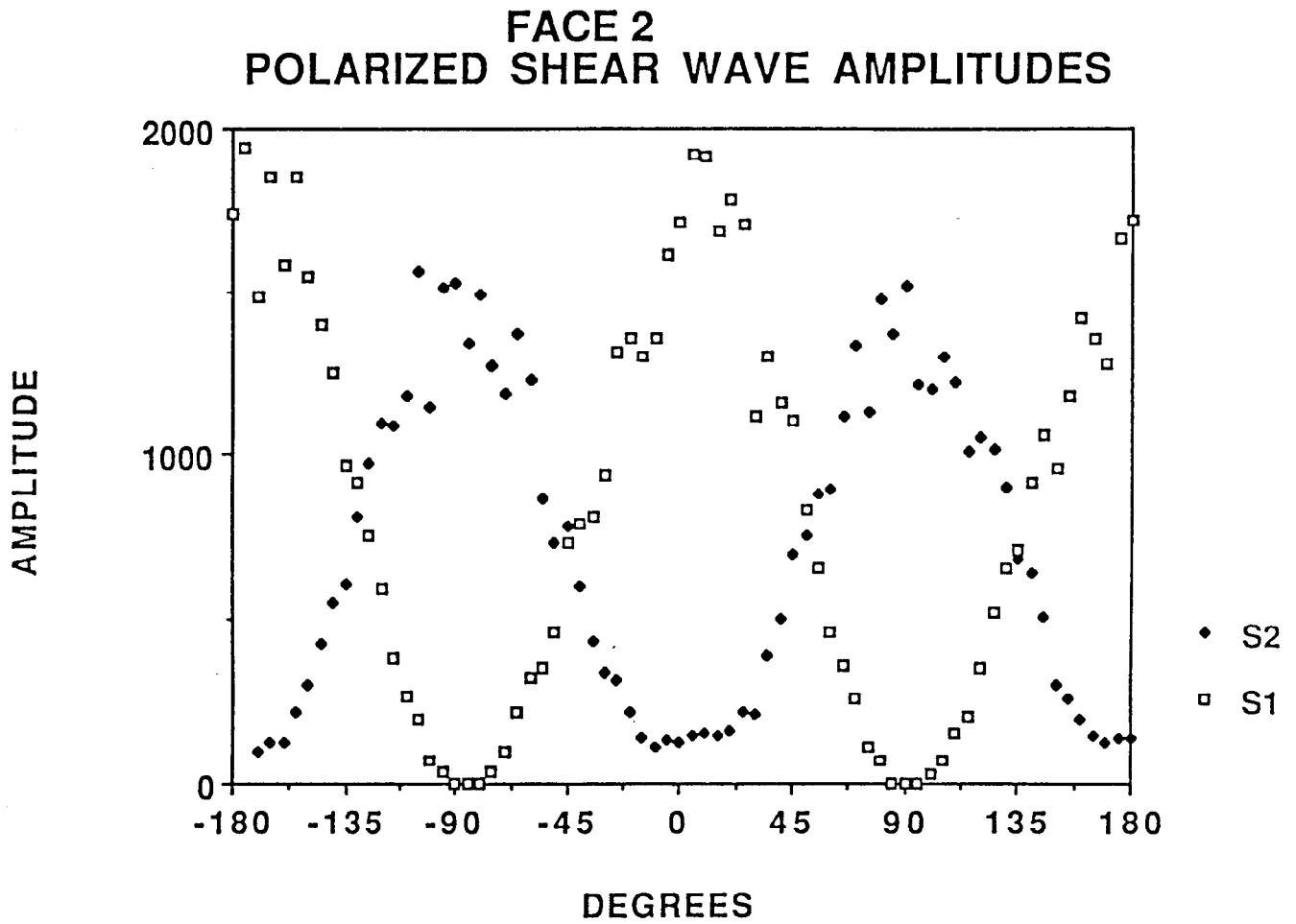


Fig. 6. The plot of amplitude vs. azimuth with respect to the polarization direction of the shear-wave transducers for a record through Face 2. The scatter of the measured amplitudes from the sinusoidal variation with azimuth is due to variable coupling of the transducers to the sample during rotation.

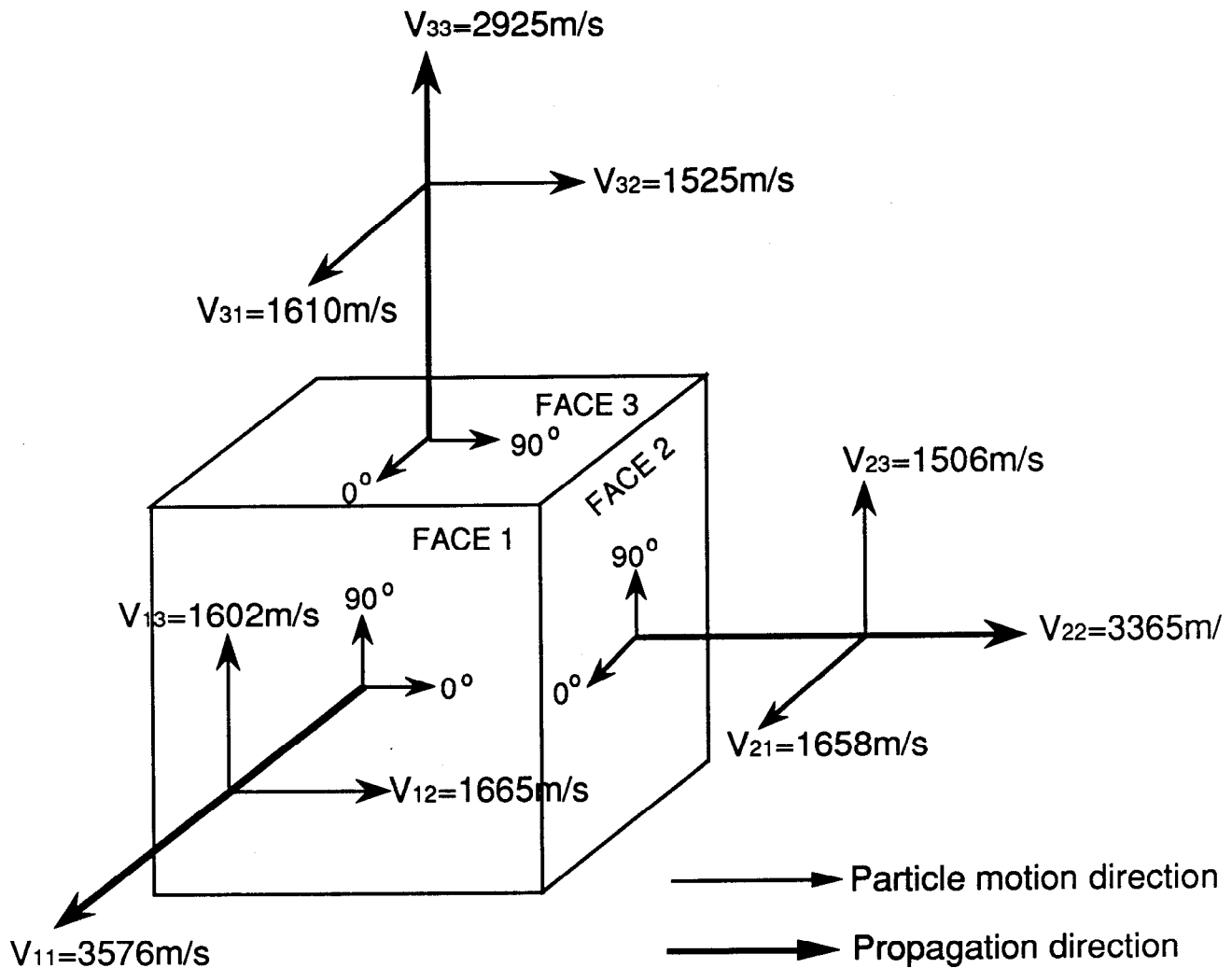


Fig. 7. The measured P-wave and S-wave velocities measured along the principal axes are summarized, with the heavy arrow designating the direction of propagation and the lighter arrow the direction of particle motion of the shear waves. The subscripts correspond to the directions of propagation and particle motion respectively. Of the six shear wave velocities, three distinct pairs of values are recognized.

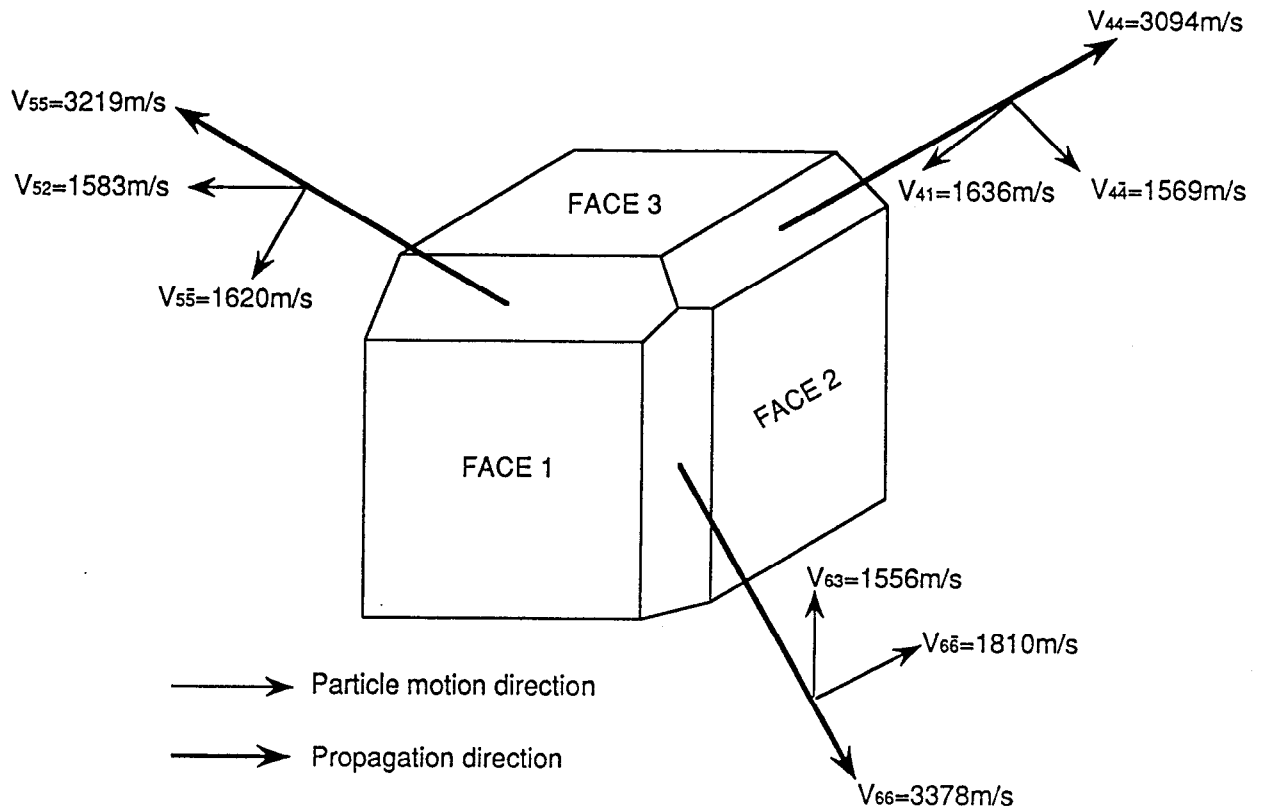


Fig. 8. The results of transmission measurements between opposing edges of the phenolic cube are summarized. The propagation directions were at 45° to two of the principal axes and perpendicular to the third.

accuracy, we also observed only three different *S*- wave velocities among the six measured for axial propagation. The shear-wave velocities may be paired as follows:

- 1) propagation in the medium direction and particle motion in the slow direction, or vice versa (i.e.  $V_{23} \approx V_{32}$ );
- 2) propagation in the fast direction and particle motion in the slow direction, or vice versa (i.e.  $V_{13} \approx V_{31}$ );
- 3) propagation in the medium direction and particle motion in the fast direction, or vice versa (i.e.  $V_{21} \approx V_{12}$ ).

Each of the velocities along the diagonal raypaths is the average of two measurements (between the two pairs of opposing edges of the cube) which had equivalent raypaths relative to the principal axes within each of the three principal planes. The two traveltimes for each of the diagonal raypath pairs were virtually identical, differing by 2 sample points (100 ns) or less in all cases. Four measurements were also recorded for raypaths from corner to corner of the cube, with similarly small differences in the velocities. This symmetry confirmed that the principal planes do correspond to the directions of the orthogonal weave of fibers and the planar layering of the canvas fabric in the phenolic, as assumed.

### ORTHORHOMBIC ANISOTROPY

For orthorhombic symmetry, it is required that  $V_{12} = V_{21}$ ,  $V_{31} = V_{13}$  and  $V_{23} = V_{32}$ , all of which are satisfied by the observed shear-wave velocities along the principal axes. Three distinct compressional velocities were measured in mutually orthogonal directions. The results of the transmission experiments indicate that the orthorhombic symmetry system is appropriate to describe the anisotropy of this material. Following the indicial notation used by Thomsen (1986), and assuming the summation convention, stress  $\sigma$  and strain  $\epsilon$  are related by

$$\sigma_{ij} = C_{ijkl} \epsilon_{kl}, \quad i, j = 1, 2, 3. \quad (1)$$

For the case of orthorhombic symmetry, the 3x3x3x3 stiffness tensor  $C_{ijkl}$  may be reduced to a 6x6 symmetric matrix

$$C_{mn} = \begin{bmatrix} C_{11} & C_{12} & C_{13} & & & \\ & C_{22} & C_{23} & & & \\ & & C_{33} & C_{44} & & \\ & & & & C_{55} & \\ & & & & & C_{66} \end{bmatrix} \quad (2)$$

of nine independent coefficients (Nye, 1985). Using the elastic equations of motion the stiffnesses  $C_{mn}$  may be estimated from the observed body-wave velocities and the density of the phenolic as outlined in the Appendix. The results of the stiffness computations are summarized in Table 1. The equations of motion involve phase velocities, while the observations are of group velocities. Along the principal axes, the phase and group velocities are equal, and the stiffnesses were computed directly using equations (A-45) and (A-46). Along the diagonal raypaths, because the wavefront is not in general spherical, the direction of the wavefront normal (i.e. the slowness direction) is not necessarily the same as the 45° direction of the raypath (i.e. of energy transport).

TABLE 1. BODY-WAVE VELOCITIES AND STIFFNESS COEFFICIENTS

MODE	GROUP VELOCITY (m/s)	PHASE VELOCITY (m/s)	PHASE ANGLE (deg.)	STIFFNESS COEFFICIENT ( $\times 10^9$ N/m <sup>2</sup> )
<b>RAYPATHS IN PRINCIPAL DIRECTIONS</b>				
P V <sub>33</sub>	2925			C <sub>33</sub> 11.670
P V <sub>22</sub>	3365			C <sub>22</sub> 15.445
P V <sub>11</sub>	3576			C <sub>11</sub> 17.443
S V <sub>21</sub>	1658 1662			C <sub>66</sub> 3.768
S V <sub>12</sub>	1665 (avg)			
S V <sub>31</sub>	1610 1606			C <sub>55</sub> 3.518
S V <sub>13</sub>	1602 "			
S V <sub>32</sub>	1525 1516			C <sub>44</sub> 3.135
S V <sub>23</sub>	1506 "			
<b>RAYPATHS AT 45° TO PRINCIPAL DIRECTIONS</b>				
P V <sub>66</sub>	3378	3373	41.6	C <sub>21</sub> 7.225 7.341
SV V <sub>66</sub>	1810	1809	47.1	C <sub>2I</sub> 7.457 (avg)
SH V <sub>63</sub>	1556	1556	48.3	
P V <sub>55</sub>	3219	3155	33.4	C <sub>13</sub> 7.451 7.230
SV V <sub>55</sub>	1620	1620	45.0	C <sub>13</sub> 7.008 "
SH V <sub>52</sub>	1583	1577	39.8	
P V <sub>44</sub>	3094	3066	37.1	C <sub>23</sub> 6.630 6.645
SV V <sub>44</sub>	1569	1569	45.7	C <sub>23</sub> 6.660 "
SH V <sub>41</sub>	1636	1632	47.0	

TABLE 2. MEASURED ANISOTROPY

	$\delta$	$\epsilon$	$\gamma$
21-plane	-0.047	0.063	0.059
31-plane	0.183	0.224	0.096
32-plane	0.081	0.150	0.035

Furthermore, for a particular  $45^\circ$  raypath, the  $P$ ,  $SV$  and  $SH$  modes have, in general, different slowness directions. The procedure used to compute these directions, the phase velocities and the related stiffnesses for the diagonal raypaths is described in the Appendix.

Nine independent velocity values are required to enable complete determination of the stiffness matrix for the case of orthorhombic anisotropy. These could include the three  $P$ -wave velocities along the principal axes, three shear-wave velocities (one of each pair, or their average) also along the principal axes, and three  $P$ -wave or  $SV$ -wave velocities, each for a raypath perpendicular to one and at  $45^\circ$  to the other two principal axes. In principal, measurements at other orientations could be used but these would require considerably more complex solutions.

Since we actually observe more than nine velocities, the internal consistency of the orthorhombic symmetry model can be checked. For example, the averages of the shear-wave velocity pairs for propagation along the principal axes (see Figure 7) were used to calculate model  $SH$ -mode velocities along the diagonal raypaths (see Figure 8), i.e.,

$$\begin{aligned} V'_{41} &= \sqrt{2} V_{13}V_{12} / (V_{13}^2 + V_{12}^2)^{1/2} \\ &= 1633 \text{ m/s} . \end{aligned} \quad (3)$$

The observed  $V_{41}$  value is 1636 m/s, a difference of 0.18%. Similarly,  $V'_{52} = 1583$  m/s, equal to the observed value, and  $V'_{63} = 1559$  m/s, differing by 0.19% from the observed  $V_{63}$  value of 1556 m/s. Clearly, the  $SH$ -mode velocities observed along the diagonal raypaths conform very well to the assumed orthorhombic symmetry model. The stiffness coefficients off the diagonal of the matrix, i.e.  $C_{12}$ ,  $C_{31}$  and  $C_{23}$ , can be computed using either the  $P$ -wave or the  $SV$ -wave velocities from the diagonal raypaths (see Appendix A). For example, either  $V_{44}$  or  $V_{4\bar{4}}$  can be used in the computation of a value for  $C_{23}$ . Separate stiffnesses were computed using the measured  $P$ -wave and  $SV$ -wave velocities, and the results are summarized in Table 1. The largest deviation, calculated as a percentage with respect to the mean of the two coefficients, is  $\pm 3.0\%$ , and is associated with the 13-plane which exhibits the largest anisotropy. In the 12-plane and 32-plane, the relative deviations between the  $P$  and  $SV$  stiffnesses are  $\pm 1.6\%$  and  $\pm 0.2\%$  respectively.

## DISCUSSION

### Degree of anisotropy

The conventional measures of anisotropy for the transverse isotropy case are given by Thomsen (1986) as

$$\epsilon = [V_p(90^\circ) - V_p(0^\circ)] / V_p(0^\circ) \quad (4)$$

and

$$\gamma = [V_s(90^\circ) - V_s(0^\circ)] / V_s(0^\circ) . \quad (5)$$

At least in the case of transverse isotropy, the  $\epsilon$  term is not always useful in the context of the limited ray angles typical of surface seismic gathers. The term

$$\delta = 4[V_p(45^\circ)/V_p(0^\circ) - 1] - [V_p(90^\circ)/V_p(0^\circ) - 1] \quad (6)$$

was defined by Thomsen (1986) and its use in conjunction with moveout velocity and stress analysis was discussed.

The measures of these velocity ratios determined in the principal planes of the phenolic are shown in Table 2, and fall within the range of the values reported by Thomsen (1986) for a variety of rocks. The *P*-wave anisotropy ranges from 6.3% in the 21-plane to 22.4% in the 31-plane. The *SH*-wave anisotropy ranges from 3.5% in the 32-plane to 9.6% in the 31-plane. The plane of weakest *P*-wave anisotropy is not the same as the plane of weakest *SH*-wave anisotropy, but the planes of strongest anisotropy do correspond. Anisotropy of the *SV* mode is observed along the 45° raypaths. In the 12-plane,  $V_{66}$  is 1810 m/s, 8.9% higher than  $V_{21}$ . In the 32-plane,  $V_{44}$  is 1569 m/s, 3.5% higher than  $V_{32}$ . *SV* anisotropy in the 31-plane is negligible despite this plane exhibiting the strongest *P* and *SH* anisotropy.

### Origin of the anisotropy

The cause of the anisotropy in the phenolic laminate appears to be related to the layering and weave of the canvas fabric. The material behaves like a stack of nets set in a gel, with different fiber densities in the directions of the three principal axes. The many causes of anisotropy in rocks range from the microscopic to the macroscopic, including preferred orientation of mineral grains, pores or fractures (Crampin, 1981, 1984, 1985), thin-layer lamination (Helbig, 1983) and regional stress (Nikitin and Chesnokov, 1984). Anisotropy has been recognized in many rocks (Thomsen, 1986; Banik, 1984; Lewis et al., 1989; Ensley, 1989), but the physical cause and symmetry systems of specific cases of anisotropic media are seldom unambiguously identified. Transverse isotropy can be invoked for horizontal thin-bed layering, for example, in shale sequences, while azimuthal anisotropy may arise in the idealized case of aligned vertical fractures. Both of these examples would be degenerate cases of the more general orthorhombic system. Two or more sources of anisotropy superimposed orthogonally within the same lithologic unit, such as aligned vertical fracturing of a horizontally laminated sequence, could result in orthorhombic anisotropy. The phenolic laminate is being used to simulate media with similar velocity properties regardless of the different physical causes of the anisotropy.

### CONCLUSIONS

Ultrasonic modeling with Phenolic CE laminate has demonstrated the anisotropic elastic properties of the material. The patterns of shear-wave splitting observed through each face of a cube of the phenolic, along with the measured compressional-wave velocities, were used to define orthogonal principal axes related to the slow, medium and fast directions through the material. Shear- and compressional-wave velocities were also measured in directions between opposing edges and opposing corners of the cube to support the determination of the orientations of the planes of symmetry. Within a principal plane, the *SV* wave has equal velocities for propagation in either of the axial directions. Velocities computed for specific directions of propagation, based on velocities from other directions and assuming the orthorhombic model, closely matched the observed values. Analysis of the data supports the interpretation that the anisotropy conforms very closely to a system of orthorhombic symmetry.

Physical modeling is currently proceeding with the phenolic and involves the recording of shot gathers as well as simulated VSP and crosswell experiments. The effect of orthorhombic anisotropy on moveout velocities and tomographic reconstruction will be described in future reports. Physical model data using phenolic laminate should prove to be a valuable adjunct to numerical studies of the increasingly important topic of anisotropy.

### ACKNOWLEDGEMENTS

This research is supported by funding provided by the corporate sponsors of the CREWES Project at the University of Calgary. The authors also wish to acknowledge the technical contributions of Mr. Malcolm Bertram of the Department of Geology and Geophysics, University of Calgary, and Mr. Eric Gallant of the CREWES Project.

### REFERENCES

- Aki, K., and Richards, P.G., 1980, Quantitative seismology: Theory and methods: W.H. Freeman and Co.
- Banik, N.C., 1984, Velocity anisotropy of shales and depth estimation in the North Sea basin: *Geophysics*, 49, 1411-1419.
- Bullen, K.E., 1963, An introduction to the theory of of seismology: Cambridge University Press.
- Crampin, S., 1981, A review of wave motion in anisotropic and cracked elastic-media: *Wave Motion*, 3, 343-391.
- 1984, An introduction to wave propagation in anisotropic media: *Geophys. J. Roy. Astr. Soc.*, 76, 17-28.
- 1985, Evaluation of anisotropy by shear-wave splitting: *Geophysics*, 50, 142-152.
- 1989, Suggestions for a consistent terminology for seismic anisotropy: *Geophysical Prospecting*, 37, 753-770.
- Ebrom, D.A., Tatham, R.H., Sekharan, K.K., McDonald, J.A., and Gardner, G.H.F., 1990, Hyperbolic traveltime analysis of first arrivals in an azimuthally anisotropic medium: A physical modeling study: *Geophysics*, 55, 185-191.
- Ensley, R.A., 1989, Analysis of compressional- and shear-wave seismic data from the Prudhoe Bay Field: *The Leading Edge*, 8, no. 11, 10-13.
- Fedorov, F.I., 1968, Theory of elastic waves in crystals: Plenum Press.
- Helbig, K., 1983, Elliptical anisotropy - its significance and meaning: *Geophysics*, 48, 825-832.
- Keith, C.M., and Crampin, S., 1977, Seismic body waves in anisotropic media: Reflection and refraction at a plane interface: *Geophys. J. Roy. Astr. Soc.*, 49, 181-208.
- Kendall, J-M., and Thomson, C.J., 1989, A comment on the form of the geometrical spreading equations, with some numerical examples of seismic ray tracing in inhomogenous, anisotropic media: *Geophys. J. Int.*, 99, 401-413.
- Lewis, C., Davis, T.L., Vuillermoz, C., Gurch, M., Iverson, W., and Schipperijn, A.P., 1989, Three-dimensional imaging of reservoir heterogeneity, Silo Field, Wyoming: Expanded Abstracts from SEG 59th Annual International Meeting and Exposition, 763-765.
- Liu, E., Crampin, S., and Booth, D.C., 1989, Shear-wave splitting in cross-hole surveys: modeling: *Geophysics*, 54, 57-65.
- Musgrave, M.J.P., 1970, Crystal acoustics: Holden-Day.
- Nikitin, L.V., and Chesnokov, E.M., 1984, Wave propagation in elastic media with stress-induced anisotropy: *Geophys. J. Roy. Astr. Soc.*, 76, 129-133.
- Nye, J.F., 1985, Physical properties of crystals: Oxford University Press.
- Tatham, R.H., Matthews, M.D., Sekharan, K.K., Wade, C.J., and Liro, L.M., 1987, A physical model study of shear-wave splitting and fracture intensity: Expanded Abstracts from SEG 57th Annual International Meeting and Exposition, 642-645.
- Thomsen, L., 1986, Weak elastic anisotropy: *Geophysics*, 51, 1954-1966.
- 1988, Reflection seismology over azimuthally anisotropic media: *Geophysics*, 53, 304-313.
- Vlaar, N.J., 1968, Ray theory for an anisotropic inhomogenous elastic medium: *Bull. Seis. Soc. Am.*, 58, 2053-2072.
- Yale, D.P., and Sprunt, E.S., 1989, Prediction of fracture direction using shear acoustic anisotropy: *The Log Analyst*, March-April, p. 65-70.

## APPENDIX

### RELATIONSHIPS AMONG VARIOUS ELASTIC-WAVE PARAMETERS IN AN ANISOTROPIC MEDIUM OF ORTHORHOMBIC SYMMETRY

#### Basic theory and the Kelvin-Christoffel equations

The equations of motion governing wave propagation in a generally isotropic elastic medium are given by many authors (e.g. Bullen, 1963; Fedorov, 1968; Musgrave, 1970; Aki and Richards, 1980; Crampin, 1981, 1984; Nye, 1985). For infinitesimal displacements  $u_i$ , Cartesian coordinates  $x_i$ , density  $\rho$ , stress tensor  $\sigma_{ij}$  and body forces per unit mass  $g_i$ :

$$\rho \ddot{u}_i = \sigma_{ij,j} + \rho g_i \quad (\text{A-1})$$

where,  $j$  denotes the partial derivative with respect to  $x_j$  and where the Einstein summation convention (for repeated indices) applies.

The stress tensor, in terms of the strain tensor  $\epsilon_{kl}$  and the stiffness tensor  $C_{ijkl}$ , is given in accordance with Hooke's law by:

$$\sigma_{ij} = C_{ijkl} \epsilon_{kl} \quad (\text{A-2})$$

where

$$\epsilon_{kl} = \frac{1}{2} (u_{l,k} + u_{k,l}) . \quad (\text{A-3})$$

Substituting (A-2) and (A-3) into (A-1), neglecting any body forces, yields:

$$C_{ijkl} u_{k,lj} - \rho \ddot{u}_i = 0 . \quad (\text{A-4})$$

These equations of motion, and their solution for monochromatic plane-wave motion, are considered by many authors (e.g. Fedorov, 1968; Musgrave, 1970; Keith and Crampin, 1977; Aki and Richards 1980; Crampin, 1981, 1984) but here we follow Musgrave's treatment most closely.

We assume harmonic plane-wave displacement, expressed as:

$$u_k = A p_k \exp [i \omega (s_r x_r - t)] \quad (\text{A-5})$$

where  $A$  is the amplitude factor,  $p_k$  is the unit polarization (or particle displacement) vector,  $\omega$  is angular frequency,  $s_r$  is the slowness vector, and in this equation only,  $i = \sqrt{-1}$ . The slowness vector gives the direction of the wavefront normal and may further be written:

$$s_r = v^{-1} n_r \quad (\text{A-6})$$

where  $v$  is phase velocity and  $n_r$  is the unit slowness (or wavefront-normal) vector. From equation (A-4), (A-5) and (A-6) one obtains:

$$(C_{ijkl} n_j n_l - \rho v^2 \delta_{ik}) p_k = 0. \quad (\text{A-7})$$

Thus, the determination of the details of the wave motion has been cast as an eigenvalue problem in which, having specified  $C_{ijkl}$  (the stiffnesses of the medium) and  $n_r$  (the direction of phase propagation), one can solve for  $p_k$  (the particle motion or polarization vector) and three values (in general) for  $v$  (phase velocity).

Due to the well known symmetries involved (see e.g. Musgrave, 1970; Nye, 1985)

$$C_{ijkl} = C_{ijlk} = C_{jikl} = C_{klji} \quad (\text{A-8})$$

and therefore the matrix  $(C_{ijkl} n_j n_l - \rho v^2 \delta_{ik})$  is symmetric. This implies in turn that the three eigenvalues obtained for  $\rho v^2$  by setting

$$|C_{ijkl} n_j n_l - \rho v^2 \delta_{ik}| = 0 \quad (\text{A-9})$$

will be real. (Throughout this appendix vertical bars denote *determinant*).

A further consequence of the symmetries embodied in (A-8) is that there are only 21 independent stiffnesses,  $C_{ijkl}$ . Following e.g. Musgrave, (1970); Nye (1985) and Thomsen (1986), the fourth-order stiffness tensor may be written as a second-order (6x6) symmetric matrix:

$$C_{ijkl} \rightarrow C_{mn}$$

where

$$\left. \begin{aligned} m &= i && \text{if } i = j, \\ m &= 9 - (i + j) && \text{if } i \neq j \end{aligned} \right\} \quad (\text{A-10})$$

and  $n$  and  $kl$  are analogous to  $m$  and  $ij$ .

By introducing the so called Kelvin-Christoffel stiffnesses, given by Musgrave (1970) as:

$$\Gamma_{ik} = C_{ijkl}n_jn_l \quad (\text{A-11})$$

equations (A-7) and (A-9) may be rewritten as:

$$\begin{bmatrix} \Gamma_{11} - \rho v^2 & \Gamma_{12} & \Gamma_{13} \\ \Gamma_{21} & \Gamma_{22} - \rho v^2 & \Gamma_{23} \\ \Gamma_{31} & \Gamma_{32} & \Gamma_{33} - \rho v^2 \end{bmatrix} \begin{bmatrix} p_1 \\ p_2 \\ p_3 \end{bmatrix} = 0. \quad (\text{A-12})$$

and

$$\begin{vmatrix} \Gamma_{11} - \rho v^2 & \Gamma_{12} & \Gamma_{13} \\ \Gamma_{21} & \Gamma_{22} - \rho v^2 & \Gamma_{23} \\ \Gamma_{31} & \Gamma_{32} & \Gamma_{33} - \rho v^2 \end{vmatrix} = 0. \quad (\text{A-13})$$

Equations (A-12) and (A-13) are known as the Kelvin-Christoffel equations.

In the case of orthorhombic symmetry only 9 of the, in general, 21 independent stiffnesses,  $C_{mn}$ , are nonzero. The six independent Kelvin-Christoffel stiffnesses are then:

$$\begin{aligned}
 \Gamma_{11} &= n_1^2 C_{11} + n_2^2 C_{66} + n_3^2 C_{55} \\
 \Gamma_{22} &= n_1^2 C_{66} + n_2^2 C_{22} + n_3^2 C_{44} \\
 \Gamma_{33} &= n_1^2 C_{55} + n_2^2 C_{44} + n_3^2 C_{33} \\
 \Gamma_{23} &= n_2 n_3 (C_{23} + C_{44}) \\
 \Gamma_{31} &= n_3 n_1 (C_{31} + C_{55}) \\
 \Gamma_{12} &= n_1 n_2 (C_{12} + C_{66}) .
 \end{aligned}
 \tag{A-14}$$

### Propagation along a principal direction

For a slowness vector in the 1-direction,

$$n_j = (1, 0, 0) \tag{A-15}$$

and equations (A-14) reduce to:

$$\begin{aligned}
 \Gamma_{11} &= C_{11} \\
 \Gamma_{22} &= C_{66} \\
 \Gamma_{33} &= C_{55} \\
 \Gamma_{23} &= \Gamma_{31} = \Gamma_{12} = 0 .
 \end{aligned}
 \tag{A-16}$$

Equation (A-12) then becomes:

$$\begin{bmatrix}
 \Gamma_{11} - \rho v^2 & 0 & 0 \\
 0 & \Gamma_{22} - \rho v^2 & 0 \\
 0 & 0 & \Gamma_{33} - \rho v^2
 \end{bmatrix}
 \begin{bmatrix}
 p_1 \\
 p_2 \\
 p_3
 \end{bmatrix}
 = 0 .
 \tag{A-17}$$

For this rather simple case, that of propagation along a principal direction, there are three obvious eigenvalues which will zero the determinant of the 3x3 matrix. For each of these, the associated eigenvector  $p_k$  is the polarization (or unit-particle-displacement) vector.

**The P wave.** - Choosing the eigenvalue solution:

$$\Gamma_{11} - \rho v^2 = 0 \quad (\text{A-18})$$

reduces the three equations of (A-17) to two, namely:

$$\begin{bmatrix} C_{66} - C_{11} & 0 \\ 0 & C_{55} - C_{11} \end{bmatrix} \begin{bmatrix} p_2 \\ p_3 \end{bmatrix} = 0. \quad (\text{A-19})$$

The only permissible solution to (A-19) is:

$$p_2 = p_3 = 0 \quad (\text{A-20})$$

since otherwise at least two of the six independent stiffnesses would have to be equal, violating the assumption of orthorhombic symmetry. It follows from equations (A-16), (A-18) and (A-20) that

$$p_k = (1, 0, 0) \quad \text{and} \quad v_{11} = (C_{11}/\rho)^{1/2} \quad (\text{A-21})$$

where  $v_{11}$  denotes that  $v$  which applies for propagation (slowness) in the 1-direction with particle motion (polarization) in the 1-direction, that is, the  $P$ -wave velocity.

**The  $S$  waves.** - Choosing each of the other two eigenvalue solutions leads to the two solutions:

$$p_k = (0, 1, 0) \quad \text{and} \quad v_{12} = (C_{66}/\rho)^{1/2} \quad (\text{A-22})$$

and

$$p_k = (0, 0, 1) \quad \text{and} \quad v_{13} = (C_{55}/\rho)^{1/2}, \quad (\text{A-23})$$

these representing  $S$  waves polarized in the 2- and 3-directions, respectively.

The corresponding velocities and polarizations for propagation in the 2- and 3-directions are obtained from equations (A-21), (A-22) and (A-23) by cyclic variation of the indices (1, 2, 3) and of the indices (4, 5, 6). Since, for these axial propagation directions, the wavefront normal and the raypath have the same direction, one could replace  $v$  (phase) with  $V$  (group) in equations (A-21), (A-22) and (A-23).

### Propagation at 45° to two principal axes or "edge to edge"

Equation (A-21) to (A-23) and their cyclically varied analogs allow one to determine the six stiffnesses along the diagonal of the  $C_{mn}$  matrix from velocities measured along

principal directions. In order to determine the three independent off-diagonal stiffnesses, one must measure velocities for raypaths along different directions. The next simplest directions to consider would seem to be those in principal planes at  $45^\circ$  to each of two principal directions. We have measured velocities along each such raypath for the three different polarizations.

Unfortunately, the raypath or group-velocity direction is not, in general, the same as the wavefront-normal or phase-velocity direction (Figure A-1). So we cannot make simple substitutions for  $n_i$  ( $= 0$  or  $\sqrt{2}/2$ ) in equations (A-14). We need additional equations that will allow determination of  $n_i$  and  $v$  from knowledge of  $\xi_i$  (the unit vector in the group-velocity direction; (Figure A-1).

Such theory has been dealt with in several works (e.g. Vlaar, 1968; Musgrave, 1970; Kendall and Thomson, 1989). Here we take the result from Musgrave (1970) and refer the reader to the works cited for details. Starting from the geometrical relationships (Figure A-1):

$$v/V = \cos \Delta = n_i \xi_i, \quad (\text{A-24})$$

Musgrave (1970, p. 89) gives

$$V_i = \frac{1}{2\rho v} \left[ \frac{p^2}{\alpha^2} \right]_k \left[ (\rho v^2 - A) \frac{\partial \alpha^2}{\partial n_i} + \alpha^2 \frac{\partial A}{\partial n_i} \right]_k \quad (\text{A-25})$$

where

$$\alpha_k = \left[ \frac{\Gamma_{ik} \Gamma_{jk}}{\Gamma_{ij}} \right]^{\frac{1}{2}}, \quad i \neq j \neq k \quad (\text{A-26})$$

and

$$A_k = \Gamma_{kk} \quad (\text{no summation}). \quad (\text{A-27})$$

In equation (A-25),  $p$ ,  $\alpha$  and  $A$  inside brackets should be represented by their  $k$ th components and the products of the brackets are summed. This notation follows Musgrave (1970) except that we use  $\xi_i$  as the unit vector whereas Musgrave uses  $\xi_i$  as the group-velocity vector, for which we use  $V_i$ .

For a medium of orthorhombic symmetry, we get from equations (A-26), (A-27) and (A-14):

$$\alpha_1^2 = n_1^2 \frac{(C_{12} + C_{66})(C_{31} + C_{55})}{(C_{23} + C_{44})} \quad (\text{A-28})$$

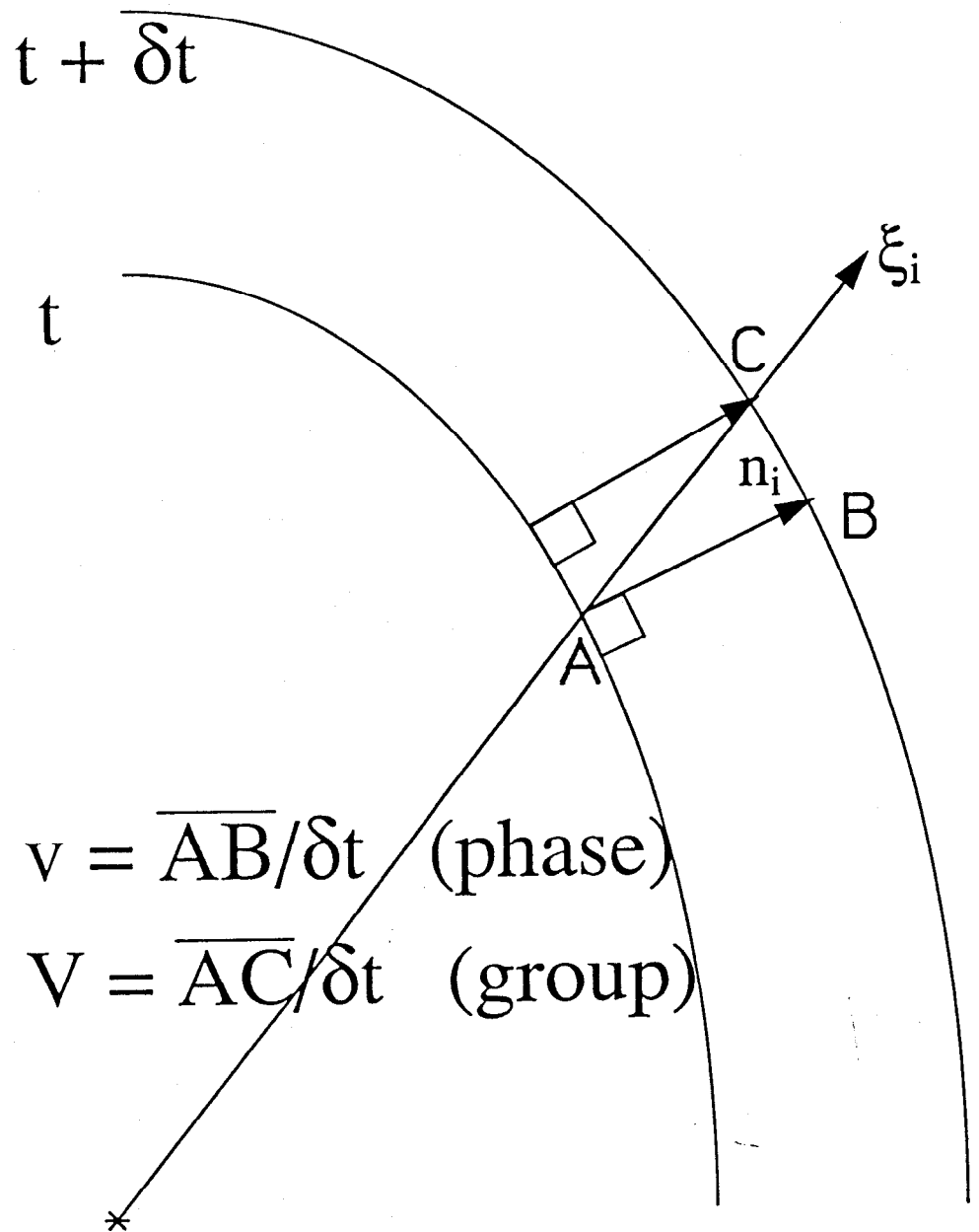


Fig. A-1. Schematic diagram of a wavefront in an anisotropic medium at times  $t$  and  $t + \delta t$ , showing the directions of the phase and group velocities,  $v$  and  $V$  respectively, and their corresponding unit vectors,  $n_i$  and  $\xi_i$  respectively.

and

$$A_1 = n_1^2 C_{11} + n_2^2 C_{66} + n_3^2 C_{55} \quad (\text{A-29})$$

and similarly for  $k = 2$  and  $3$ . Substitution into (A-24) results in:

$$\rho v V_1 = p_1^2 [(\rho v^2 - n_1^2 C_{11} - n_2^2 C_{66} - n_3^2 C_{55}) n_1^{-1} + n_1 C_{11}] + n_1 (p_2^2 C_{66} + p_3^2 C_{55}) \quad (\text{A-30})$$

and similarly for  $i = 2$  and  $3$ . If we consider propagation in the 23-plane of symmetry:

$$n_1 = 0 \text{ and } V_1 = 0. \quad (\text{A-31})$$

Thus, from equation (A-30)

$$p_1^2 n_1^{-1} (\rho v^2 - n_2^2 C_{66} - n_3^2 C_{55}) = 0. \quad (\text{A-32})$$

and therefore either

$$p_1 = 0 \quad (\text{A-33})$$

or

$$\rho v^2 = n_2^2 C_{66} + n_3^2 C_{55}. \quad (\text{A-34})$$

**The quasi- $P$  and - $SV$  waves.** – Equation (A-33) implies polarization entirely within the 23-plane (the sagittal plane), i.e.  $P$ - $SV$  types. From the analogs to equation (A-30) for  $i = 2$  and  $3$  we then get:

$$\rho v V_2 = p_2^2 n_2^{-1} (\rho v^2 - n_3^2 C_{44}) + p_2^2 n_2 C_{44}$$

and

(A-35)

$$\rho v V_3 = p_2^2 n_3 C_{44} + p_3^2 n_3^{-1} (\rho v^2 - n_2^2 C_{44}).$$

Further, from equation (A-12) for this case we get:

$$\frac{p_2}{p_3} = \frac{n_2 n_3 (C_{23} + C_{44})}{\rho v^2 - n_2^2 C_{22} - n_3^2 C_{44}} = \frac{\rho v^2 - n_2^2 C_{44} - n_3^2 C_{33}}{n_2 n_3 (C_{23} + C_{44})} \quad (\text{A-36})$$

from which

$$\frac{p_2^2}{p_3^2} = \frac{\rho v^2 - n_2^2 C_{44} - n_3^2 C_{33}}{\rho v^2 - n_2^2 C_{22} - n_3^2 C_{44}} \quad (\text{A-37})$$

Since the raypath or group-velocity direction is at  $45^\circ$  to the 2- and 3-axes,  $V_2 = V_3$  and the two right-hand sides of equations (A-35) are equal. From this and equation (A-37) one can eliminate  $p_2$  and  $p_3$  and obtain:

$$\begin{aligned} \rho^2 v^4 (n_3 - n_2) + \rho v^2 [n_2^3 (C_{22} + C_{44}) - n_3^3 (C_{33} + C_{44})] \\ + C_{33} C_{44} n_3^4 (n_2 + n_3) - C_{22} C_{44} n_2^4 (n_2 + n_3) = 0. \end{aligned} \quad (\text{A-38})$$

It is clear from (A-36) that there are two solutions for  $v^2$  and thus for  $p_2/p_3$ . One of these solutions is the quasi- $P$  or  $qP$ -wave case, the other the  $qSV$ -wave case. For  $qP$  we denote the phase velocity  $v_{44}$  and the group velocity  $V_{44}$ . For  $qSV$  these are  $v_{4\bar{4}}$  and  $V_{4\bar{4}}$ , respectively. There is, it is true, a fundamental incongruity between the single- and double-subscript notations for  $V$ . However, we do not try to combine the two and thus no problem ever arises here.

Defining  $\theta = \cos^{-1} n_3$ , we can write (Figure A-1) that  $\Delta = \theta - 45^\circ$ . Therefore, from equation (A-24) for  $qP$ :

$$v_{ij} = V_{ij} \cos \Delta = (\sqrt{2}/2) (n_2 + n_3) V_{ij} \quad (\text{A-39})$$

where  $ij = 44, 4\bar{4}$  or  $41$ , for  $qP, qSV$  or  $SH$ , respectively. Using equations (A-21) to (A-23) and their cyclic variants to eliminate stiffnesses, and (A-39) to eliminate  $v$  from (A-38), we obtain:

$$\begin{aligned} V_{44}^4 (n_2 + n_3)^2 (n_3^2 - n_2^2) + 2V_{44}^2 (n_2 + n_3) [n_2^3 (V_{22}^2 + V_{23}^2) - n_3^3 (V_{33}^2 + V_{23}^2)] \\ + 4 (n_3^4 V_{33}^2 V_{23}^2 - n_2^4 V_{22}^2 V_{23}^2) = 0, \end{aligned} \quad (\text{A-40})$$

in which all of the  $V_{ij}$  have been measured experimentally. Now, since  $n_2^2 + n_3^2 = 1$ , equation (A-40) can, in principle, be solved for  $n_2$  and  $n_3$ . In practice, we determine  $n_2$  and  $n_3$  by iterative substitution. Knowing  $n_2$  and  $n_3$  and getting  $v_{44}$  from equation (A-39), equations (A-36) and (A-37) can be solved for  $C_{23}$  and the polarization,  $p_2/p_3$ . Similarly, using  $V_{4\bar{4}}$  ( $qSV$ ) in (A-40), we will get different values (in general) for  $n_2, n_3$  and  $v_{4\bar{4}}$ ; but assuming the orthorhombic model to be a reasonable one, we should get about the same result for  $C_{23}$ .

**The  $SH$  wave.**- Choosing equation (A-34) instead of (A-33) we have, from (A-14) and (A-31):

$$\rho v_{41}^2 = n_2^2 C_{66} + n_3^2 C_{55} = \Gamma_{11} \quad (\text{A-41})$$

so that the Kelvin-Christoffel equations (A-12) result in

$$p_k = (1, 0, 0) . \quad (\text{A-42})$$

Incorporating (A-31) and (A-42) into (A-30) and its cyclic variants yields:

$$\rho v_{41} V_2 = n_2 C_{66} \quad \text{and} \quad \rho v_{41} V_3 = n_3 C_{55} . \quad (\text{A-43})$$

Again applying  $V_2 = V_3$  (for rays at  $45^\circ$ ) and equation (A-39), we obtain:

$$\frac{n_2}{n_3} = \frac{C_{55}}{C_{66}} \quad \text{and} \quad V_{41} = \frac{\sqrt{2} V_{31} V_{12}}{(V_{31}^2 + V_{12}^2)^{1/2}} . \quad (\text{A-44})$$

### Expressions for stiffnesses in terms of group velocities

For completeness, expressions for the nine stiffnesses, for the case of orthorhombic symmetry, are here summarized. These equations follow directly from (A-21) to (A-23), (A-36) and (A-39), as well as their cyclic variants.

$$\left. \begin{aligned} C_{11} &= \rho V_{11}^2 \\ C_{22} &= \rho V_{22}^2 \\ C_{33} &= \rho V_{33}^2 \end{aligned} \right\} \quad (\text{A-45})$$

$$\left. \begin{aligned} C_{44} &= \rho V_{23}^2 = \rho V_{32}^2 \\ C_{55} &= \rho V_{31}^2 = \rho V_{13}^2 \\ C_{66} &= \rho V_{12}^2 = \rho V_{21}^2 \end{aligned} \right\} \quad (\text{A-46})$$

$$C_{23} = \frac{\rho}{n_2 n_3} \left\{ \left[ \frac{1}{2} (n_2 + n_3)^2 V_{44}^2 - n_2^2 V_{23}^2 - n_3^2 V_{33}^2 \right] \left[ \frac{1}{2} (n_2 + n_3)^2 V_{44}^2 - n_2^2 V_{22}^2 - n_3^2 V_{23}^2 \right]^{1/2} - \rho V_{23}^2 \right\} , \quad (\text{A-47a})$$

$$C_{31} = \frac{\rho}{n_3 n_1} \left\{ \left[ \frac{1}{2} (n_3 + n_1)^2 V_{55}^2 - n_3^2 V_{31}^2 - n_1^2 V_{11}^2 \right] \left[ \frac{1}{2} (n_3 + n_1)^2 V_{55}^2 - n_3^2 V_{33}^2 - n_1^2 V_{31}^2 \right]^{1/2} - \rho V_{31}^2 \right\} , \quad (\text{A-47b})$$

$$C_{12} = \frac{\rho}{n_1 n_2} \left\{ \left[ \frac{1}{2} (n_1 + n_2)^2 V_{66}^2 - n_1^2 V_{12}^2 - n_2^2 V_{22}^2 \right] \right. \\ \left. \left[ \frac{1}{2} (n_1 + n_2)^2 V_{66}^2 - n_1^2 V_{11}^2 - n_2^2 V_{12}^2 \right]^{1/2} - \rho V_{12}^2 \right\} \quad (\text{A-47c})$$

And in (A-47)  $V_{ii}$  ( $i = 4, 5, 6$ ) may be replaced by  $V_{ii}^*$ .